Journal of New Materials for Electrochemical Systems 18, 225-230 (2015)

A Heterojunction Based on Macro-porous Silicon and Zinc Oxide for Solar Cell Application

N. Mendoza-Agüero[1], V. Agarwal[2], H.I.Villafán-Vidales[1], J. Campos-Alvarez[1] and P.J. Sebastian[1,*]

[1]Instituto de Energías Renovables-UNAM, Temixco, Morelos 62580, México
[2]Centro de Investigación en Ingeniería y Ciencias Aplicadas-UAEM Av. Universidad 1001, Cuernavaca, Morelos, México.

Received: September 27, 2015, Accepted: October 30, 2015, Available online: November 29, 2015

Abstract: *Transparent and conductive Al doped zinc oxide (AZO) films were reactively sputtered from metallic targets onto macro-porous silicon (MPS) substrate to fabricate a heterojunction interface structure. A tungsten oxide (WO_3) thin film was placed between metallic aluminum back contact and bulk silicon to extract photogenerated holes from the absorber. Due to the susceptibility of PS to naturally oxidize over the period of time, a thin film of SiO_2 was thermally grown to stabilize the electrical response of the junction. Such thin layer acts as passive film to prevent recombination and is placed between the p-n junction. Photovoltaic properties of this heterojunction were studied by using the current density-voltage (J-V) measurement under AM 1.5 illumination. The experimental results show an increase in photovoltaic performance of AZO/MPS solar cell with a buffer layers of WO_3. Such heterostructures are promising for the development of the low-cost, clean, and durable devices with appreciable light-to-electricity conversion efficiency.*

Keywords: Heterojunction, solar cell, macro-porous silicon, zinc oxide, tungsten oxide.

1. INTRODUCTION

Zinc oxide (ZnO) is a promising transparent (>80% transmitance) conductive material for silicon based solar cells because it possesses a direct wide band gap with energy of ~3.37 eV at room temperature [1]. So far, various preparation methods have been used to fabricate ZnO films, such as: RF magnetron sputtering [2], spray pyrolysis [3], chemical vapor deposition (CVD) [4], pulsed laser deposition [5], sol–gel process [6], thermal evaporation [7], reactive evaporation [8] and screen printing [9]. Among these techniques RF Sputtering has been the most suitably used because it allows work at low temperatures and gives deposits of better adhesion and higher density than other methods. Moreover, thin films with a wide band gap, high transparency and low resistivity, such as ZnO, are required as window material for solar cells to be suitable for solar energy conversion. Such band gaps of these materials are large enough to be transparent to most of the useful solar spectra, and the resistivity is small enough to avoid series resistance effects. In several photovoltaic devices, ZnO films are used not only as a window material but also as a p–n heterojunction partner [10-12].

Optical loss minimization is one of the major goals in photovoltaic systems in the improvement of solar cell efficiency. As it is known, bare silicon has been shown to be capable of absorbing only ~70% of the useful incident solar radiation [13]. These reflection losses are generally minimized by the use of anti-reflection (AR) coatings. The materials which have been widely used for AR coatings have important disadvantages such as the requirement of multiple depositions, thus increasing the fabrication costs. [14-17].

Porous silicon exhibits direct band-gap behavior with low production cost and an easy fabrication material compatible with silicon solar cell technology. In this particular case, the possibility of modulating the refractive index attracts the attention of researchers to use it in photovoltaic technology. Several studies have proposed the use of PS as single or multilayer AR coatings [18–22].

PS samples can be easily fabricated by electrochemical anodization of crystalline silicon in a fluorine-containing electrolyte [23].

In the visible region, an increase in porosity generates a low refractive index and high absorption coefficient [24]. Thus, a highly porous layer can enhance the efficiency of solar cells by increasing light trapping into the active region [23], can be used as ARC to serve as path centers and reduce the impurity levels of the

*To whom correspondence should be addressed: Email: sjp@ier.unam.mx

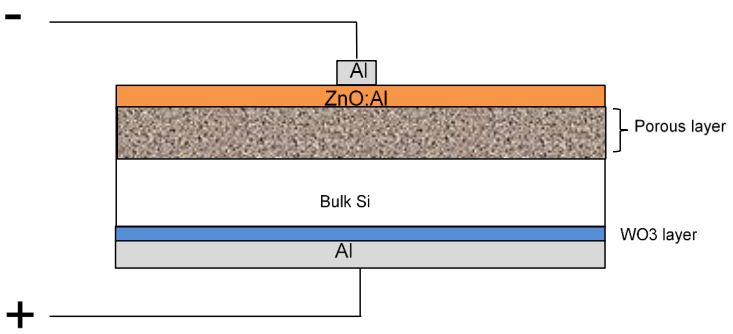

Figure 1. Schematic drawing of solar cell configuration based on porous silicon showing the buffer layer of tungsten oxide.

Si substrate [25] and, finally, it absorbs more light energy in crystalline silicon solar cells [26].

The use of porous silicon (PS) in solar cell technology is not new. For the first time, considerable capacity of PS as promising material for photovoltaics was promoted in early 90's [27-29]. In these investigations, the principles and advantages of PS for solar cells application were formulated, proceeding from the analysis of microstructure and properties of this material. Recently, encouraging results have been reported by Salman et. al. [30] who produced 1 cm^2 circular area Si solar cells with PS ARC by anodization; an efficiency of 15.5% is reported.

In addition, reports on ZnO films deposited on PS for solar cell application was never reported. However there are several works based on ZnO/cristalline-Si heterojunctions [31-34]. Also, composites based on PS and ZnO has been already reported [35-38]. In such investigations the characterization in terms of diode applications was roughly studied, however the behavior under light illumination is not presented.

In this work we report the fabrication of p-n heterojunction between Al-doped ZnO (AZO) thin films and macro-porous silicon substrates, using a WO_3 to prevent electron leakage and to aid in the hole extraction. The properties such as the current–voltage measurements were characterized.

2. EXPERIMENT DETAILS

2.1. Preparation of Macro Porous Silicon

MPS was formed by an electrochemical etching of (100)-oriented, boron-doped p-type silicon substrates of resistivity 14–22 □□cm, using an electrolyte consisting of 4 M hydrofluoric acid (48 wt%) in N'N-Dimethylformamide (ACS reagent, ≥99.8%). Anodization time was kept at 10 min and current density as 12 mA/cm^2. After fabrication, the samples were rinsed with DMF and dried with slow nitrogen flux. We used a double sided polished silicon wafer and the area of the Teflon® electrochemical cell was 0.8 cm^2. Evaporated Al back contact was used to ensure uniform current distribution.

2.2. Deposition of ZnO

ZnO:Al thin films were RF sputter-deposited on the macro porous silicon substrate at room temperature using a target (Kurt J. Lesker, 99.99% purity) in an Ar gas flux. RF power was 280 W and the base pressure inside the chamber was pumped down to less than $2.4x10^{-5}$ Torr. The deposition time for all the films was 35 min, so that the film deposition rates could then be determined. Also AZO films were grown on glass substrates for other optical characterizations and over crystalline silicon for comparison purposes. Finally Al metal film was deposited with a shadow mask on the AZO/MPS surface for the top electrode.

2.3. Preparation of solar WO_3

Tungsten trioxide was synthesized at high temperature by using concentrated solar radiation supplied by a 30 kW solar furnace. Commercial electrodes of pure tungsten (Weld500, purity 94%) were used as raw material. These electrodes were placed inside a reaction chamber designed to work at high temperatures (800 °C) and concentrated solar energy. A rotary vacuum pump was connected at the bottom of the cavity in order to ensure continuous inert gas flow (Ar and O_2). During experimentation, the chamber was operated for direct normal irradiation above 900 W/m^2 and pressures of 0.8 bar. At the end of experimentation, it was obtained yellow crystals on the tungsten surface that were analyzed by X-ray diffraction.

2.4. Deposition of WO_3

Prior to fabrication of photovoltaic device a thin film of WO_3 was thermally evaporated at high vacuum ($3.4x10^{-5}$ mbar) onto the backside of polished silicon wafer. Ultimately, a 1 □m Al film was deposited, by high vacuum evaporation, on the top of WO_3 layer to ensure an optimum back ohmic contact.

AZO films were deposited on to MPS substrates in a Dual Source Sputtering and Evaporation (MVSystems, Inc.). WO_3 films and front/back were deposited on the backside of bulk silicon, by evaporation in a Coating System (Balzers, BAE 250). Crystalline properties of the AZO films were investigated using X-ray diffraction (XRD) Rigaku diffractometer with Cu αK1.54 radiation (Mod. DMAX-2200, calibrated with LaB6). Scanning Electron Microscopy (FE-SEM S-550, ITACHI Co.) was used to study the surface morphology of the films. Also, the cross-section of film thickness is observed by using SEM. Optical reflectance and transmittance of AZO films were acquired with UV–vis spectroscopy (Shimadzu Spectrophotometer 3101 PC) in the wavelength range 250–2500 nm. The current density -voltage characteristics (J–V) of the heterojunctions were measured by using a DC voltage–current source unit. The electrical resistivity of the AZO films was measured by dc 2 electrode-4 terminal method.

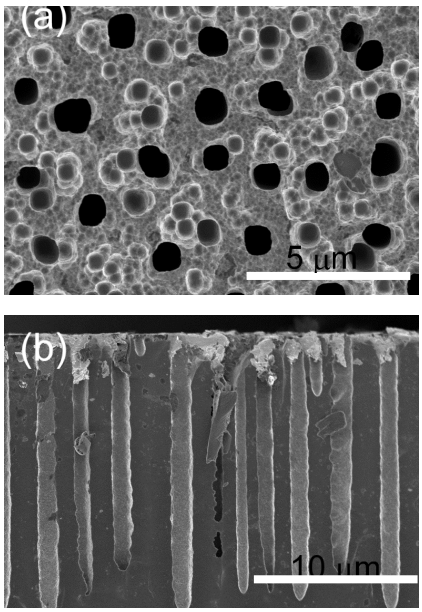

Figure 2. Macroporous silicon etched for 10 min at 12 mA/cm^2. (a) Plan view and (b) cross-sectional view.

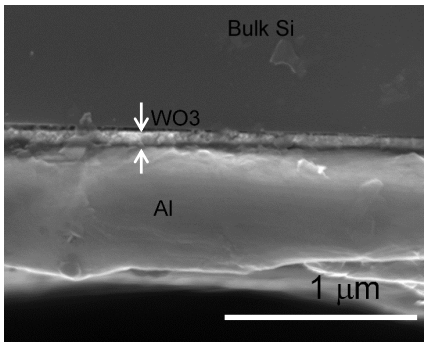

Figure 3. Cross-sectional view of the back ohmic contact showing the buffer layer of WO_3.

3. RESULTS AND DISCUSSION

Figure 1 shows the configuration of photovoltaic device based on macroporous silicon and Al doped zinc oxide. Prior to anodization of crystalline silicon, a thin film of resistive WO_3 was evaporated on the backside of polished silicon wafer. Immediately after, a thick layer of aluminum metal was deposited over the buffer layer.

The sample is heated at 500 °C for 20 min under N_2 atmosphere to ensure an optimum ohmic contact. Al back contact is useful in anodization of bulk silicon since it helps current to flow through the electrochemical cell and to create a uniform porous layer. After PS fabrication a thin film of AZO was deposited by RF Sputtering and then annealing at 550 C for 1 h in a mixture of H_2(5%)-N_2 ambient to form p-n junction. This annealing process is necessary to generate a stable p-n heterojuction. In this work, samples without annealing lacks the response under solar irradiation. Finally Al front contact is sputtered using a mask to obtain a 3 mm diameter

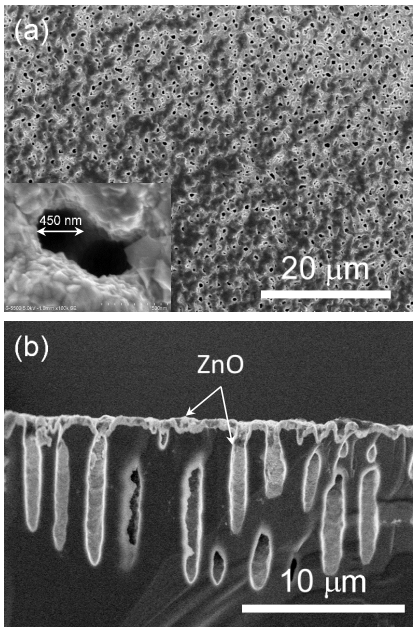

Figure 4. Morphology of Al doped zinc oxide layer covering macroporous silicon surface. (a) Plan view and (b) cross-sectional view.

circle, then annealed at 500 °C for 30 min under N_2 atmosphere.

Top and cross sectional SEM micrographs of MPS samples as obtained from the anodic etching process are depicted in Figure 2. The pores were 500-750 nm diameter approximately circular in cross section and reasonably uniform over large areas. These images reveal a uniform surface and squared/rounded (Fig. 2a). Cross-sectional SEM data indicated that the pores were approximately the same length across a given sample, with only minimal branching (Figure 2b). The silicon wafers were etched for 10 min for the formation of ~15 μm thick porous layer.

Tungsten oxide layers were deposited by evaporation on the back polished side of silicon wafers between Al contact and bulk silicon. Figure 3 displays a constant thickness of ~70 nm for WO_3 resistive film followed by a thick Al layer of 600-750 nm. Those samples are annealed at 500 °C for 20 min at N_2 conditions.

Figure 4 shows the morphology of ZnO:Al films deposited and heated at 550 °C onto MPS substrates. A porous ZnO:Al surface is observed (Fig. 4a) covering almost one half of the hole pore (inset Fig. 4a). Thickness of this layer is about ~600 nm as it can be seen in SEM micrographs from electron backscatter diffraction (Fig. 4b). Shining zone represents Zn metal and dark zone silicon material. It is observed that ZnO:Al material is adhered to the walls of the pore. EDS analysis demonstrated, taken from 600 nm thickness of ZnO:Al layer, a percentage atomic composition of 54.13 % corresponding to oxygen, 43.46 % to zinc, 1.74% silicon and 0.67% aluminum. By the other side, an EDS measurement inside the pore displays the following atomic composition: oxygen (0.78%), silicon (99.07) and zinc (0.15%); aluminum is undetectable at this point (Fig. 4b).

The high atomic percentage of silicon is understandable since one is employing Si substrate for the heterostructure. The electron beam hits the surface of the sample in radial direction instead of

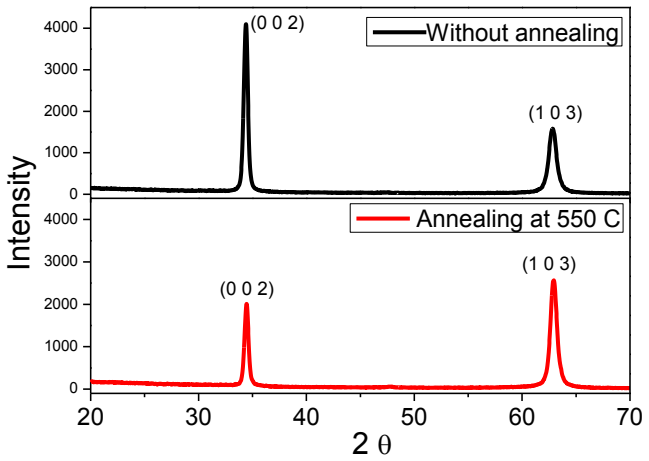

Figure 5. XRD patterns of the Al doped ZnO films deposited by rf puttering (a) at room temperature and (b) annealed at 550 C for 1h.

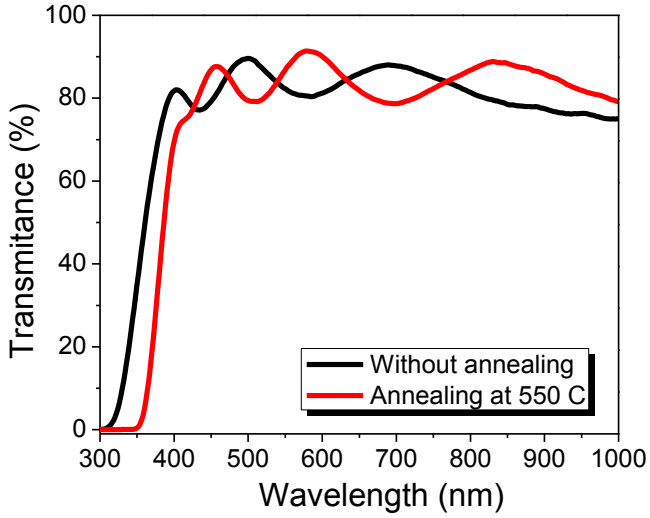

Figure 6. Transmission spectra of ZnO thin film grown on glass.

perpendicular direction. Radial beam covers the great silicon surface and hence measures only a small portion of ZnO inside the pores. Also, one can appreciate that ZnO films contain only low content of oxygen which means there are vacancies inside ZnO matrix.

Figure 5 shows XRD spectra of Al doped ZnO film on glass, which was deposited by RF Sputtering on a glass substrate. The XRD pattern of ZnO phase was in agreement with published pdf data number 36-1451 for synthetic zincite. It is documented that under ambient conditions the thermodynamically stable phase of zinc oxide is zincite that crystallizes in the hexagonal wurtzite (ZnS, space group $P6_3mc$) structure.

The peak located at 34.4 is attributed to the ZnO:Al (002) diffraction. The results indicate that the ZnO:Al has a hexagonal wurtzite structure with its dominant film orientation along the c-axis perpendicular to the substrate surface. No diffraction peaks of Al or other impurity phases are detected in these samples. One can

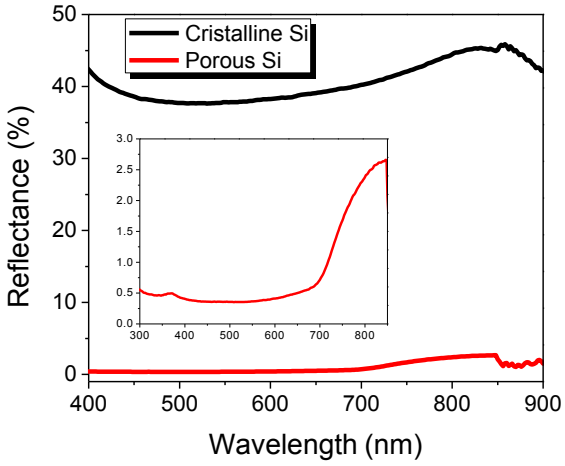

Figure 7. Reflectance spectra of a as prepared macroporous (inset) silicon and cristallline silicon.

observe that in annealed sample the ecristallinity slightly increases and it was found a preferential orientation along (103) planes in contrast to those samples under heat treatment.

The optical properties of Al doped ZnO films are presented in Figure 6. The films without annealing and annealed at 550 °C have an average transmission of 84% and 83% over the 400–800 nm range respectively, including all reflection losses and absorption in the glass substrate. Sharp absorption spectra is observed at around the cut-off wavelengths, which implies that the ZnO:Al has the direct energy bandgap. The high optical transmittance allow the ZnO films to be suitable for the application as window materials for solar cells.

Thin absorber layers require an efficient light trapping for a sufficiently high optical absorption. Therefore, optical reflection was measured on MPS samples. The average effective reflectivity (400–700 nm) of square shaped macroporous samples was 38.7% and 0.42% for crystalline Si and MPS, respectively (Fig. 7). Note that MPS samples are without an additional anti-retlection coating. These results on monocrystalline Si show that, in order to obtain the lowest reflectivity, it is necessary to fabricate porous Si.

Figure 8a shows the output characteristics of a crystalline silicon-ZnO:Al solar cell without SiO_2 passive layer and WO_3 buffer layer for comparison. The dark current density-voltage (*J-V*) curve of the device shows *J-V* characteristics similar to those of an ideal diode [36, 38]. Under illumination, the device exhibits a low open circuit voltage (V_{oc}) of 204 mV, and a short circuit current density (J_{sc}) of 0.0000113 mA/cm^2. When porous Si is introduced, current density shows an increase of four orders of magnitude (Fig. 8b): 0.037 mA/cm^2, meanwhile V_{oc} increases slightly to 220 mV. As it can be observed, MPS layer enhances the performance of the device, due to its antireflection properties and Al doped ZnO layer acting as a window. SiO_2 thin layer was thermally grown over MPS at 80 °C and 5 min under oxygen ambient in a hermetic oven. The aim of SiO_2 layer is to passivate the interface. By inserting a buffer layer of resistive WO_3, V_{oc} values are higher about 250 mV and short circuit current density of 0.9 mA/cm^2 (Fig. 9) increasing these values about one order of magnitude. Such WO_3 film prevents interface recombination due to convenient HOMO position extracting

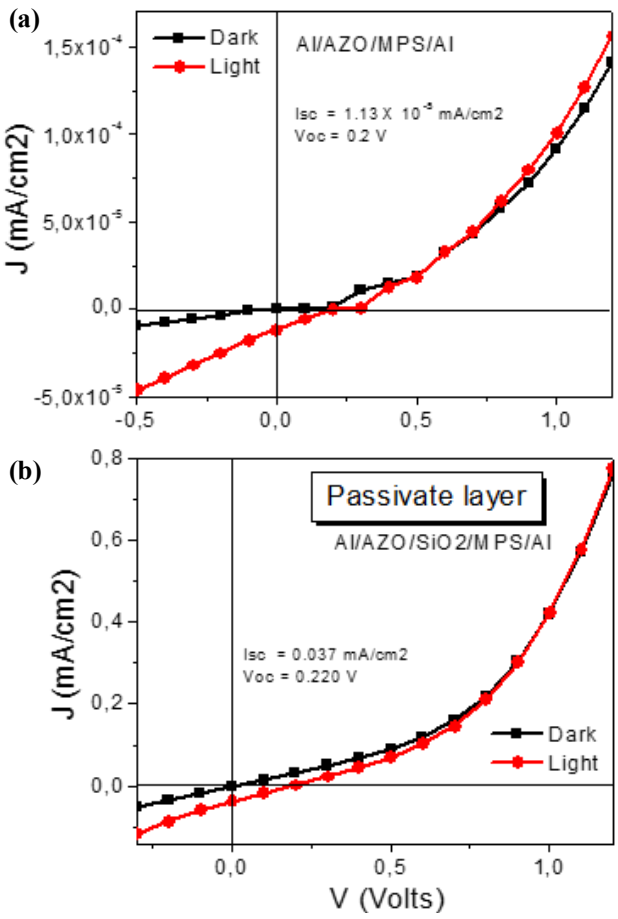

Figure 8. (a) J-V curves for ZnO:Al-crystalline silicon solar cells in the dark and under AM1.5 illumination. (b) J-V curves for solar cells with ZnO:Al-MPS configuration.

photogenerated holes at the bulk Si/Al interface. The high work function of WO_3 (-4.8 eV) will enhance hole collection at the photoactive layer/Ag interface.

With these studies we demonstrated that, by inserting resistive SiO_2 and WO_3 layers photovoltaic performance improvement has reached and, thus represent a meritorious and viable approach for efficient solar conversion. We expect device optimization (e.g., trapping light into the device), surface passivation, and better contacts for further enhancement to the performance of the ZnO:Al/MPS configuration.

4. CONCLUSIONS

In summary, we have demonstrated the fabrication of a new configuration of solar cell consisting of macro porous/Al doped ZnO heterojunction. A SiO_2 thin film was inserted at the p-n junction in order to passivate porous surface and prevent recombination. Along with that, a WO3 buffer layer was placed between the active layer and back Al electrode which prevents recombination due to a hole extraction, leading to the improvement of J_{sc} and V_{oc}. Current density increased about five orders of magnitude by incorporating WO3 buffer layer.

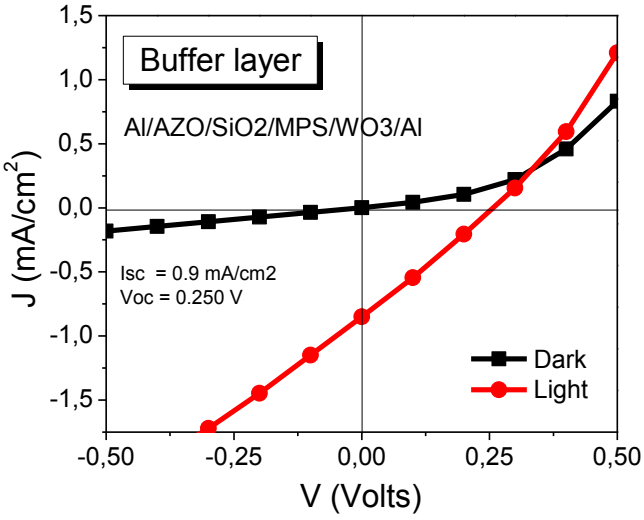

Figure 9. J–V characteristic of the $ZnO/SiO_2/MPS/WO_3$ heterojunction in dark and in light under AM1.5 illumination.

5. ACKNOWLEDGEMENTS

The authors appreciate the technical support received from Miss Maria Luisa Ramon and Mr. Gildardo Casarubias. This work was supported through the grants IT100413 and CONACYT 236978.

REFERENCES

[1] A.B. Djurisic, Mater. Sci. & Eng., B38, 237 (2002).
[2] H. Czternastek, Opto-Electronics Review, 12, 49 (2004).
[3] T. Prasada Rao, T and Santhoshkumar, Appl. Surf. Sci., 255, 4579 (2009).
[4] S.T. Tan, B.J. Chen, X.W. Sun, W.J. Fan, H.S. Kwok, X.H. Zhang, S.J. Chua, J. Appl. Phys., 98, 013505 (2005).
[5] R.K. Shukla, A. Srivastava, K.C. Dubey, J. Crystal Growth, 294, 427 (2006).
[6] Young-Sung Kim, Weon-Pil Tai, Appl. Surf. Sci., 253, 4911 (2007).
[7] P. Teesetsopon, S. Kumar, J. Dutta, Int. J. Electrochem. Sci., 7, 4988 (2012).
[8] G. Gordillo, C. Calderón, Solar Energy Materials & Solar Cells, 69, 251 (2001).
[9] Q. Qi, T. Zhang, Q. Yu, R. Wang, Y. Zeng, L. Liu, H. Yang, Sensors and Actuators B, 133, 638 (2008).
[10]W. Zhang, Q. Meng, B. Lin, Z. Fu, Solar Energy Materials & Solar Cells, 92, 949 (2008).
[11]X.M. Zhang, D. Golberg, Y. Bando, N. Fukata, Nanoscale, 4, 737 (2012).
[12]Y.F. Zhu, D.H. Fan, Y.W. Dong, G.H. Zhou GH, Superlattices and Microstructures, 74, 261 (2014).
[13]F. Chen F, L. Wang, Light Trapping Design in Silicon-Based Solar Cells, Solar Cells - Silicon Wafer-Based Technologies, Prof. Leonid A. Kosyachenko (Ed.), ISBN: 978-953-307-747-5, InTech, 2011.

[14]Sang-Hun Jeong , Jae-Keun Kim , Bong-Soo Kim , Seok-Ho Shim , Byung-Teak Lee, Vacuum 76, 507 (2004).
[15]K. Lucas, O. Adetutu, C.C. Hobbs, Y. Musgrove, Yeong-Jyh Tom Lii, US Patent 6,004,850, (1999).
[16]M. Cid, N. Stem, C. Brunetti, A.F. Beloto, C.A.S. Ramos, Surface and Coatings Technology, 106 117 (1998).
[17]S.E. Lee, S.W. Choi, J. Yi, Thin Solid Films, 376, 208 (2000).
[18]M. Lipinski, P. Panek, Z. Siwatek, E. Beltowska, R. Ciach, Solar Energy Materials & Solar Cells, 72, 271 (2002).
[19]C.S. Solanki, R.R. Bilyalov, J. Poortmans, J. Nijs, R. Mertens, Solar Energy Materials & Solar Cells, 83, 101 (2004).
[20]H. Nouri, M. Bouaicha, B. Bessais, Solar Energy Materials & Solar Cells, 93, 1823 (2009).
[21]E. Osorio, R. Urteaga, L.N. Acquaroli, G. García-Salgado, H. Juárez, R.R. Koropecki, Energy Materials & Solar Cells, 95, 3069 (2011).
[22]A. Ramizy, W.J. Aziz, Z. Hassan, K. Omar, K. Ibrahim, Optik, 122, 2075 (2011).
[23]O. Bisi, S. Ossicini, L. Pavesi, Surface Science Reports, 38, 1 (2000).
[24]L. Santinacci, A.M. Gonçalves, N. Simon, A. Etcheberry, Electrochim. Acta, 56, 878 (2010).
[25]Y.S. Tsuo, J.R. Pitts, M.D. Landry, P. Menna, C.E. Bingham, A. Lewandowski, T.F. Ciszek, Sol. Energy Mater. Sol. Cells, 41-42, 41 (1996)
[26]W.A. Badawy, R.M. El-Sherif, S.A. Khalil, Electrochim. Acta, 55, 8563 (2010).
[27]G. Smestad, M. Kunst, C. Vial, Solar Energy Materials and Solar Cells, 26, 277 (1992).
[28]Y.S. Tsua, Y. Xiao, M.J. Heben, X. Wu, F.J. Pern, S.K. Deb, Proceedings of 23rd IEEE Photovoltaic Specialists Conference, IEEE, 287-293 (1993).
[29]Y.S. Tsuo, M.J. Heben, X. Wu, Y. Xiao, C.A. Moore, P. Verlinden, S.K. Deb, Proceedings of MRS Symposium, 283, 405 (1993).
[30]K.A. Salman, Z. Hassan, K. Omar, Int. J. Electrochem. Sci., 7, 376 (2012).
[31]H. Zhu, J. Hupkes, E. Bunte, J. Owen, S. Huang, Solar Energy Materials & Solar Cells, 95, 964 (2011).
[32]Xiao-Mei Zhang, D. Golberg, Y. Bando, N. Fukata, Nanoscale, 4, 737 (2012).
[33]R. Pietruszka, G. Luka, K. Kopalko, E. Zielony, P. Bieganski, E. Placzek-Popko, M. Godlewski, Mater. Sci. in Semiconductor Proc., 25, 190 (2014).
[34]Arpita Jana, Siddhartha Ghosh, P. Sujatha Devi, Nil Ratan Bandyopadhyay, Mallar Ray, J. Mater. Chem. C, 2, 9613 (2014).
[35]O. Marin, G. Grinblat, A.M. Gennaro, M. Tirado, R.R. Koropecki, D. Comedi, Superlattices and Microstructures, 79, 29 (2015).
[36]R.G. Singh, F. Singh, I. Sulania, D. Kanjilal, K. Sehrawat, V. Agarwal, R.M. Mehra, Nuclear Instruments and Methods in Physics Research Section B: Beam Interactions with Materials and Atoms, 267, 2399 (2009).
[37]X.L. Huang, S.Y. Ma, L.G. Ma, H.Q. Bian, C. Su, Physica E: Low-dimensional Systems and Nanostructures, 44, 190 (2011).
[38]Y. Kumar, M. Herrera, F. Singh, S.F. Olive-Méndez, D. Kanjilal, S. Kumar, V. Agarwal, Materials Science and Engineering: B, 177, 1476 (2012).